

## Article

# Gold Nanoparticles as Monoanion Sensors through Modified Electrophilicity

Almudena Martí <sup>1,\*</sup>, Pau Arroyo <sup>2,3</sup>, Pablo Gaviña <sup>2,3,4</sup>, Salvador Gil <sup>2,3,4</sup>, Margarita Parra <sup>1,2,3,4</sup> and José A. Sáez <sup>2,3,\*</sup>

<sup>1</sup> Faculté des Sciences et Technologies—Campus Aiguillettes, Université de Lorraine, CNRS, L2CM, UMR 7053, F-54506 Vandœuvre-lès-Nancy, France

<sup>2</sup> Instituto Interuniversitario de Investigación de Reconocimiento Molecular y Desarrollo Tecnológico (IDM), Universitat de València–Universitat Politècnica de València, Doctor Moliner 50, 46100 Burjassot, Spain; pau.arroyo@uv.es (P.A.); pablo.gavina@uv.es (P.G.); salvador.gil@uv.es (S.G.)

<sup>3</sup> Departamento de Química Orgánica, Universitat de València, Doctor Moliner 50, 46100 Burjassot, Spain

<sup>4</sup> CIBER de Bioingeniería, Biomateriales y Nanomedicina (CIBER-BBN), Av. Monforte de Lemos, 3-5, 28029 Madrid, Spain

\* Correspondence: almudena.marti-morant@univ-lorraine.fr (A.M.); jose.a.saez@uv.es (J.A.S.)

**Abstract:** Derived from malachite green, new triaryl-carbonium-ion-functionalized gold nanoparticles have been synthesized for detecting anions. The detection process, and concomitant colour change, is based on charge compensation on the surface of nanoparticles, which triggers their aggregation, resulting in a bathochromic shift of the plasmon resonance band. The difference in electrophilicity of the malachite green triaryl ions in solution or on gold nanoparticles makes it possible to distinguish different anions related to their nucleophilic character.

**Keywords:** malachite green; gold nanoparticles; anion detection; electrophilicity; nucleophilicity



**Citation:** Martí, A.; Arroyo, P.; Gaviña, P.; Gil, S.; Parra, M.; Sáez, J.A. Gold Nanoparticles as Monoanion Sensors through Modified Electrophilicity. *Colorants* **2023**, *2*, 591–600. <https://doi.org/10.3390/colorants2040030>

Academic Editor: Ermelinda M. S. Maçãas

Received: 5 September 2023

Revised: 22 September 2023

Accepted: 27 September 2023

Published: 29 September 2023



**Copyright:** © 2023 by the authors. Licensee MDPI, Basel, Switzerland. This article is an open access article distributed under the terms and conditions of the Creative Commons Attribution (CC BY) license (<https://creativecommons.org/licenses/by/4.0/>).

## 1. Introduction

Electrophilicity and nucleophilicity are key concepts in chemistry to understand reaction mechanisms and quantify their reaction rate and thus gain insight into the molecular behaviour. In 1953, Swain and Scott [1] were the first authors to attempt a systematic quantification of the nucleophilicity in  $S_N2$  reactions. They defined nucleophilicity,  $n$ , as an inherent property of a substance according to the following equation:  $\log(k/K_{H_2O}) = sn$ , where  $s$  stands for the sensitivity (specific for each electrophile). Later, in 1972, Richie introduced a new parameter,  $N^+$ , to characterize this property, which is independent of the nature of the electrophile [2]. On the other hand, in 1994, based on the reaction rates of some carbocations, and diazonium ions with  $n$ - and  $\pi$ -nucleophiles, Mayr and Patz introduced a three-parameter equation:  $\log k_{(20\text{ }^\circ\text{C})} = sN(N + E)$ , where  $k_{(20\text{ }^\circ\text{C})}$  is the second-order rate constant at  $20\text{ }^\circ\text{C}$ ,  $N$  is the nucleophilicity parameter,  $E$  is the electrophilicity parameter and  $sN$  is the nucleophile-specific sensitivity parameter (which is solvent-dependent) [3,4]. Critical dependence of several factors, such as basicity, polarizability, oxidation potential and solvation, were well confirmed. Parr et al. considered the electrophilicity concept on the basis of density functional theory (DFT) [5]. They proposed the  $\omega$  index as the measure of electrophilicity, which is directly related to the energy difference corresponding to the charge transfer process. Parr found a correlation between the index and the electron affinity of atoms and molecules. Based on this analysis, Kiyooka et al. introduced a theoretical intrinsic reactivity index (IRI). This index is valid as a single scale directed towards both electrophilicity and nucleophilicity using the energy levels of frontier molecular orbitals [6]. Table 1 shows the different parameters of some of the nucleophiles used in this study according to different scales. In consequence, there have been numerous attempts in the literature [7,8] in recent years to provide a unified theoretical framework for quantifying

electrophilicity and nucleophilicity, but unfortunately none of them have been completely successful to date.

**Table 1.** Nucleophilicity parameters, in acetonitrile, of some nucleophiles used in this study.

| Nucleophile            | Nucleophilicity Parameters |         |                |           |      |
|------------------------|----------------------------|---------|----------------|-----------|------|
|                        | n                          | N       | S <sub>N</sub> | ω/ε       | IRI  |
| HS <sup>−</sup>        | 5.1                        |         |                |           |      |
| CN <sup>−</sup>        | 5.1                        | 16.27   | 0.70           |           |      |
| Cl <sup>−</sup>        | 2.7                        | 17.20   | 0.60           | 1.74/0.37 | 0.34 |
| F <sup>−</sup>         |                            | 10.88 * | 0.83 *         | 4.52/0.45 | 0.50 |
| AcO <sup>−</sup>       | 2.7                        | 16.90   | 0.75           | 0.43/0.23 | 0.05 |
| <b>Malachite green</b> |                            | −42.0   | 0.82           |           |      |

\* 2% water.

Following our studies on the use of functionalized gold nanoparticles with triarylmethane derivatives as sensors [9], we have found an important effect of these nanoparticles in the electrophilicity of triarylmethane dyes that we want to describe here.

Triarylmethane dyes constitute a very important class of dyes that have been used in several fields, including biochemical applications [10–13], recognition of anions [14,15], cations [16,17] and neutral molecules [18], as well as pH indicators [19].

One structurally interesting class of carbocations are the 4-diakylamino arylmethane dyes. The highly electron-donating character of 4-diakylaminophenyl groups endow carbonium ions with remarkable stability in aqueous solutions. Further, steric hindrance of the aryl groups around the central carbocation results in considerably slower reaction rates with nucleophiles than those of most of other cations of similar stability [20].

Functionalized gold nanoparticles (AuNPs) have recently attracted interest in sensor applications [21–25]. Following our interest in the development of probes for the detection of anions, we have studied the use of gold nanoparticles functionalized with triarylmethane dyes as signalling systems. The sensing strategy is based on the colour change that arises from the shift in the surface plasmon resonance band that occurs during the aggregation of AuNPs or the dispersion of AuNPs aggregates. The red colour of dispersed nanoparticles turns dark blue upon aggregation and the colour change can be observed by the naked eye even at low concentrations [26,27]. Triarylmethane-functionalized AuNPs remain dispersed in solution due to the electrostatic repulsion of the cationic charges at the triaryl carbonium ions. In the presence of reactive anions, their nucleophilic addition to the electrophilic carbocations will neutralize the positive charges, triggering the aggregation process (see Figure 1).

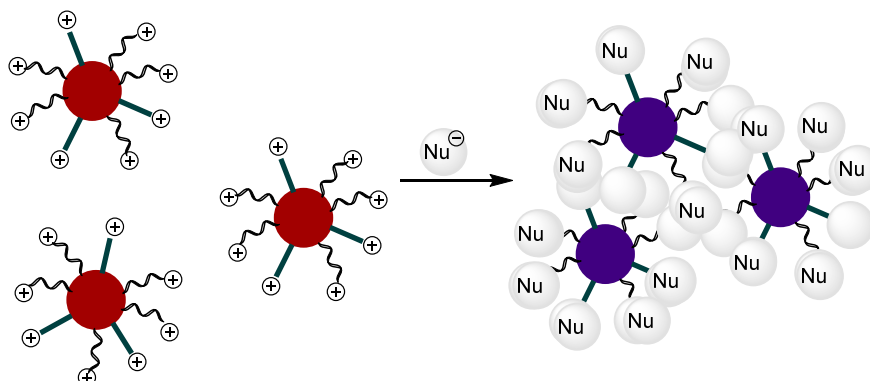


**Figure 1.** Paradigm of the sensing mechanism using triaryl-carbonium-ion-functionalized AuNPs: the nucleophilic anions react with the terminal ligands, neutralizing the positive charges and inducing the aggregation of the nanoparticles.

## 2. Materials and Methods

Hydrogen tetrachloaurate (III) tetrahydrate, *p*-bromobencylalcohol, *n*-Buli, Malachite green carbinol 90% dye, sodium citrate tribasic dyhydrate and 4,4'-bis(dimethylamino)-benzophenone were obtained from Sigma-Aldrich. NH<sub>4</sub>PF<sub>6</sub>, NH<sub>4</sub>OAc, KCN, NaCl, NaClO<sub>4</sub>, NaSH and KF were also obtained from Sigma-Aldrich.

### 2.1. General Procedures

All reagents were commercially available and were used without further purification. Silica gel 60 F<sub>254</sub> (Merck) plates were used for TLC. Milli-Q ultrapure water was used for the synthesis of the AuNPs and in the sensing experiments. <sup>1</sup>H and <sup>13</sup>C NMR spectra were recorded with a Bruker Avance 300 MHz spectrometer. Chemical shifts are reported in ppm with tetramethylsilane as an internal standard. High-resolution mass spectra were recorded in the positive ion mode with a VG-AutoSpec mass spectrometer. UV-vis absorption spectra were recorded in a 1 cm path length quartz cuvette with a Shimadzu UV-2101PC spectrophotometer. All measurements were carried out at 293 K (thermostatically controlled). Zeta potentials were measured with a Malvern Zetasizer ZS three times in 10–25 cycles. X-ray photoelectron spectroscopy (XPS) was employed to verify the success of the molecular modification of the NP surfaces. The spectra were recorded with an Escalab 210 spectrometer from Thermo VG Scientific. The base pressure in the analysis chamber was 1.010–10 mbar. Photoelectrons were extracted by using the Mg-K $\alpha$  excitation line ( $\text{hv} = 1253.6 \text{ eV}$ ). The binding energy of the spectra refers to the Fermi level. The electronic images were obtained with a JEOL-1010 transmission electron microscope operating at 100 kV. Samples were prepared for TEM characterization by applying a drop of colloidal solution to a carbon-coated copper grid.

### 2.2. Synthesis of Compound 1

Compound 1 was synthesized according to the literature [28]. The Malachite green (MG<sup>+</sup>) dye (1.6 g, 4.6 mmol) was dissolved in 15 mL of DMSO and heated to 60 °C. A concentrated HCl solution was added (10 M, 4.6 mmol) followed by the addition of KCN (0.65 g, 10 mmol), and the resulting pale solution was stirred for 10 min. The mixture was allowed to cool down to room temperature. Next, 50 mL of water was added, and the mixture was extracted with ethyl acetate (50 mL). The organic layer was washed with 50 mL of brine, dried over anhydrous MgSO<sub>4</sub> and evaporated in vacuum. The compound was purified by column chromatography (SiO<sub>2</sub>, DCM/AcOEt 9:1) and a pale green solid was obtained (1.143 g, 70%).

<sup>1</sup>H-NMR (300 MHz, CDCl<sub>3</sub>):  $\delta = 7.39\text{--}7.22$  (m, 5H), 7.07 (d,  $J = 9.1 \text{ Hz}$ , 4H), 6.68 (d,  $J = 9.03$ , 4H), 2.97 (s, 12H) ppm; <sup>13</sup>C-NMR (75.4 MHz, CDCl<sub>3</sub>):  $\delta = 150.2$ ; 142.0; 133.1; 129.8; 128.8; 128.5; 124.7; 112.3; 110.9; 44.4; 40.4 ppm.

### 2.3. Synthesis of Compound 5

In a typical run, *p*-bromobenzyl alcohol (0.187 g, 1.00 mmol) was dissolved in 20 mL of anhydrous THF under argon atmosphere. The solution was cooled to –70 °C. *n*-Butyllithium (1.0 mL of a 2.5 M solution in hexane, 2.5 mmol) was added dropwise with a syringe under continuous stirring. The mixture was left at –70 °C for 15 min. Then, 4,4'-bis(dimethylamino)-benzophenone (0.188 g, 0.7 mmol) was added as a solid under stirring, and the mixture was allowed to warm to room temperature and left for 2 h. Saturated solution of NaHCO<sub>3</sub> (50 mL) was added to quench the reaction, and ethyl acetate (50 mL) was used to extract the crude product. The organic phase was washed with 30 mL of brine and dried over anhydrous MgSO<sub>4</sub>. The insoluble solids were removed by vacuum filtration, and ethyl acetate was concentrated using a rotary evaporator. The crude product was further purified by silica gel column chromatography using hexane/ethyl acetate (1:3, *v/v*) as eluent. After removing all the solvents, the product, 4, was obtained as a green solid (0.160 g, yield: 60%).

<sup>1</sup>H-NMR (300 MHz, CDCl<sub>3</sub>): δ = 7.15 (d, J = 6.8 Hz, 2H), 7.05 (d, J = 6.8 Hz, 2H), 6.80 (d, J = 6.7 Hz, 4H), 6.63 (d, J = 6.7 Hz, 4H); 4.50 (s, 2H), 2.91 (s, 12H) ppm; <sup>13</sup>C-NMR (75.4 MHz, CDCl<sub>3</sub>): δ = 150.2; 149.6; 140.3; 135.1; 129.8; 127.8; 126.9; 113.7; 81.5; 69.4; 40.5.

A 50 mL round-bottom flask was charged with lipoic acid (0.112 g, 4.91 mmol), DCC (0.112 g, 4.91 mmol) and anhydrous DCM (20 mL). The reaction mixture was cooled to 0 °C in an ice water bath, and a solution of **4** (0.160 g, 4.25 mmol), DMAP (catalytic amount) and anhydrous CH<sub>2</sub>Cl<sub>2</sub> (25 mL) was added dropwise over a period of 1 h under magnetic stirring. After the addition was completed, the reaction mixture was stirred at 0 °C for 1 h and then allowed to warm to room temperature for 12 h. After removing the insoluble salts via vacuum filtration, the filtrate was concentrated and further purified by silica gel column chromatography using hexane/ethyl acetate (1:6, v/v) as eluent. After removing all the solvents with a rotary evaporator, the product, **5**, was obtained as a green solid (0.068 g, yield: 40%).

<sup>1</sup>H-NMR (300 MHz, CDCl<sub>3</sub>): δ = 7.25 (d, J = 8.1 Hz, 2H), 7.15 (d, J = 8.1 Hz, 2H), 6.80 (d, J = 8.0 Hz, 4H), 6.60 (d, J = 8.0 Hz, 4H), 5.05 (s, 2H), 2.90 (s, 12H), 2.5–2.3 (m, 5H), 1.80–1.60 (m, 2H), 1.55–1.45 (m, 4H), 1.42 (m, 2H) ppm; <sup>13</sup>C-NMR (75.4 MHz, CDCl<sub>3</sub>): δ = 173.8; 157.2; 150.0; 147.5; 140.5; 129.6; 129.2; 128.1; 114.1; 81.9; 66.3; 56.7; 40.9; 40.6; 38.9; 34.3; 29.1; 26.8; 25.0.

#### 2.4. Preparation of the Functionalized AuNPs: NP1

Gold nanoparticles were prepared by reducing HAuCl<sub>4</sub> with trisodium citrate. All glassware was thoroughly cleaned with freshly prepared aqua regia (HCl:HNO<sub>3</sub> in 3:1 molar ratio), rinsed thoroughly with water and dried in air. NPs with a diameter of 13 nm were synthesized as reported previously [29,30]. Briefly, 5 mL of 38.8 mM trisodium citrate solution was added into 50 mL of 1 mM HAuCl<sub>4</sub> boiling solution, and the resulting solution was then kept continuously boiling for 30 min until a red solution was obtained. The solution was cooled to room temperature, and then the mixture was filtrated through a 0.22 μm membrane filter to remove the precipitate and the filtrate was then stored in a refrigerator at 4 °C for further use. The size of NPs was measured with a transmission electron microscope. Modification of NPs through the ligand-exchange reaction was performed at room temperature by mixing 10 mL of the as-prepared NPs with 20 μL of aqueous solution of 1 mM of compound **5** in DMF. NP1 was centrifuged for 20 min (13,000 rpm) and then suspended in DMF.

### 3. Results

#### 3.1. Study of Commercial Malachite Green (MG<sup>+</sup>) Dye versus Anions in Solution

First, the behaviour of the commercial malachite green (MG<sup>+</sup>) triarylmethane dye was studied in solution. This compound has a strong absorption band in the visible region to produce intense, brilliant shades of blue-green [31]. Its absorption spectrum in DMF (Figure 2, top) is characterized by an intense absorption band at 619 nm ( $\epsilon = 62,980 \text{ cm}^{-1} \text{ mol}^{-1} \text{ L}$ ), arising from a  $\pi \rightarrow \pi^*$  transition, along with two less intense  $\pi \rightarrow \pi^*$  transitions at 420 nm ( $\epsilon = 11,440 \text{ cm}^{-1} \text{ mol}^{-1} \text{ L}$ ) and 312 nm ( $\epsilon = 11,430 \text{ cm}^{-1} \text{ mol}^{-1} \text{ L}$ ), respectively. It is well established that MG<sup>+</sup> cations react with a variety of nucleophiles (such as cyanide and bisulfide anions or amines) in different solvents following second-order kinetics [32].

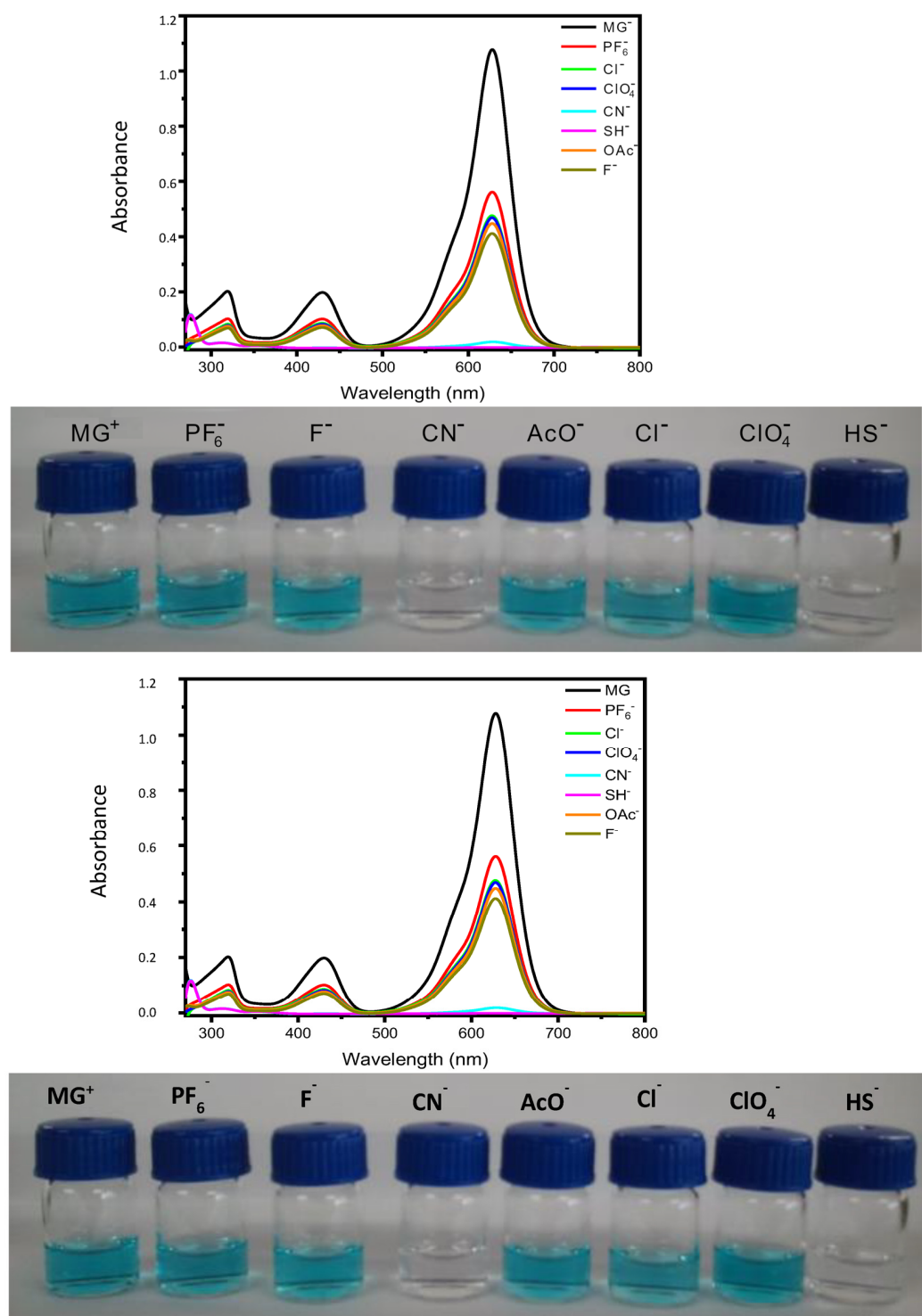
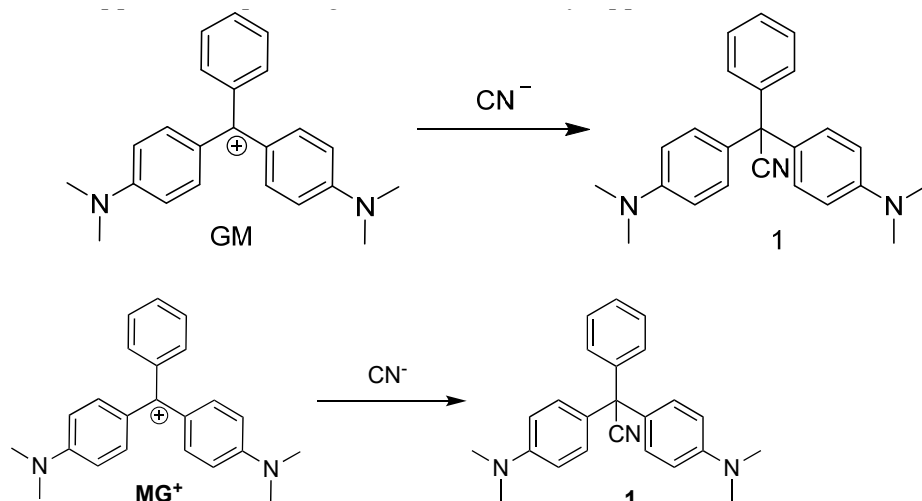


**Figure 2.** (Top) Changes in the UV-vis absorption spectrum of a solution of  $\text{MG}^+$  ( $1 \times 10^{-5}$  M) in DMF after the addition of  $200 \mu\text{L}$  of an aqueous solution of different anions ( $3 \times 10^{-3}$  M). (Bottom) Visual colour changes of DMF solutions of  $\text{MG}^+$  after the addition of different anions.

This nucleophilic addition can be easily followed by the disappearance of the main absorption bands in the visible region of the UV-vis spectra, resulting in a bleaching of the solution [33]. In fact, when aqueous solutions of different anions ( $\text{CN}^-$ ,  $\text{SH}^-$ ,  $\text{AcO}^-$ ,  $\text{F}^-$ ,  $\text{Cl}^-$ ,  $\text{ClO}_4^-$  and  $\text{PF}_6^-$ ) ( $3 \times 10^{-3}$  M) were added to a solution of  $\text{MG}^+$  in DMF ( $1 \times 10^{-5}$  M), only cyanide and bisulfide anions led to an important decrease in the intensity of the

three characteristic UV-vis absorption bands of  $\text{MG}^+$  with concomitant disappearance of the blue-green colour of the solution (see Figure 2, bottom).

The nucleophilic addition of cyanide anion to  $\text{MG}^+$  was confirmed by the independent synthesis of the corresponding leucocyanide adduct from the reaction of the carbinol derivative of  $\text{MG}^+$  with excess of  $\text{KCN}$  in acidic media (see Supplementary Materials). We envisaged that the observed colour change in the titration of  $\text{MG}^+$  with  $\text{CN}^-$  may arise from the addition reaction of  $\text{CN}^-$  at the carbocationic core, resulting in the formation of the colourless species **1** (Scheme 1). To corroborate this hypothesis, when a DMF solution of GM was reacted with an excess of  $\text{CN}^-$ , the blue-green colour of  $\text{MG}^+$  changed to colourless. To confirm the formation of **1**, the reaction was performed according to the literature [28]. Subsequent to the disappearance of the blue-green colour of  $\text{MG}^+$ ,  $^1\text{H}$  and  $^{13}\text{C}$  NMR spectra were recorded, which unequivocally confirmed the formation of **1** (see Supplementary Materials). In the  $^{13}\text{C}$  NMR spectrum, a signal at 207.1 ppm, corresponding to the carbocation, was observed. On reaction with  $\text{^7CN}$ , this signal disappeared and a signal at 110.9 ppm, corresponding to the nitrile moiety, appeared instead.



**Scheme 1.** Synthesis of compound **1**.

Figure 3 summarizes the kinetic reactivity studies of  $\text{MG}^+$  with different anions in DMF. The decrease of the characteristic absorption band of  $\text{MG}^+$  at 619 nm in the presence of  $\text{HS}^-$  was too fast to be measured.

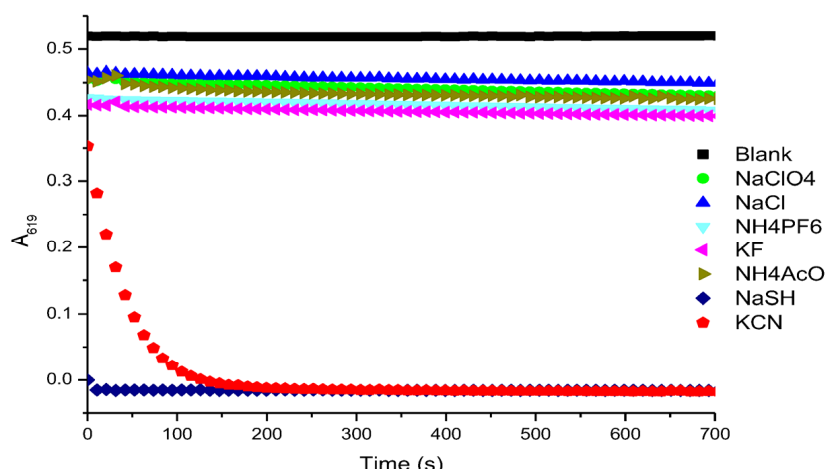
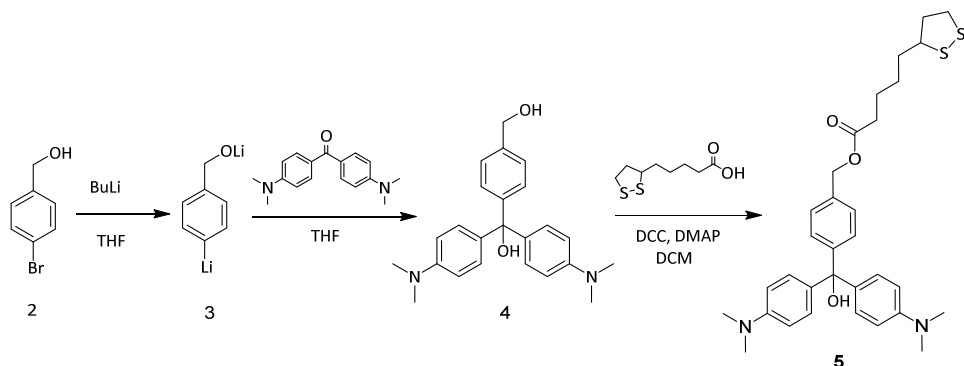


**Figure 3.** Absorption changes at 619 nm for solutions of  $\text{MG}^+$  ( $1 \times 10^{-5}$  M in DMF) after the addition of aqueous solutions of different anions (100  $\mu\text{L}$  of  $3 \times 10^{-3}$  M).

UV-vis titration studies performed with DMF solutions of  $\text{MG}^+$  in the presence of increasing amounts of  $\text{KCN}$  and  $\text{NaSH}$  showed a decrease in the intensity of the band centred at 619 nm (see Figure S2 of Supplementary Materials). In a similar trend to the kinetic study,  $\text{MG}^+$  gave a linear response from small amounts of  $\text{HS}^-$ , whereas the  $\text{CN}^-$  anion requires a threshold concentration to give a linear response.

### 3.2. Study of $\text{MG}^+$ Functionalized AuNPs versus Anions in Solution

AuNPs react easily with disulfide groups and then, for the synthesis of  $\text{MG}^+$ -functionalized AuNPs we decided to synthesize a malachite green derivative bearing an appending thioctic ester (compound 5 in Scheme 2). Thus, triarylcarbinol 4 was synthesized, in 60% yield, from 4-bromobenzyl alcohol, butyllithium and 4-(dimethylamino)benzophenone. The less hindered primary alcohol in 4 was esterified with thioctic acid in the presence of DCC and DMAP to yield compound 5 in a 40% yield after column chromatography [9]. The chemical structure and purity of 5 were confirmed by spectroscopic techniques (see Supplementary Materials). It is noteworthy that this compound did not show any absorption bands in the visible region of the UV-vis spectrum, indicating that no carbocation was generated. To generate the corresponding triaryl carbonium ion, concentrated HCl was added to DMF or acetonitrile solutions of 5, and a broad UV-vis absorption band centred at 619 nm ( $5 \times 10^{-5}$  M in DMF) was observed.



**Scheme 2.** Synthesis of  $\text{MG}^+$  derivative 5.

The functionalized AuNPs were synthesized through a two-step procedure. First, citrate-stabilized nanoparticles were prepared by reducing tetrachloroauric acid with trisodium citrate in boiling water [29,30]. Monodisperse citrate-stabilized nanoparticles were thus obtained with an average size of 13 nm, as determined by TEM. In a second step, in a ligand-exchange reaction, the citrate was replaced from the surface of the nanoparticles by cation of ligand 5. According to our experience [34], this ligand exchange does not significantly increase the size, and consequently, the typical SPR band at 530 nm appears in the UV-vis spectrum for dispersed AuNPs smaller than 25 nm. The functionalized AuNPs (NP1) were then centrifuged and re-dissolved in DMF. The concentration of NP1 was calculated to be  $1.9 \times 10^{-9}$  M from an estimated molar extinction coefficient of  $\epsilon = 2.47 \times 10^8 \text{ M}^{-1} \text{ cm}^{-1}$  [35]. These nanoparticles were neither stable in water nor in aqueous buffer solutions, probably due to a slow hydration of the triaryl carbonium ion, leading to aggregation processes.

DMF solutions of dispersed triaryl-carbonium-ion-functionalized AuNPs (NP1) exhibited the characteristic surface plasmon resonance (SPR) band at 530 nm in the UV-vis spectrum and showed a wine-red colour. Figure 4 depicts the UV-vis spectra of DMF solutions of NP1 (blank) after the addition of 300  $\mu\text{L}$  aqueous solutions ( $3 \times 10^{-3}$  M) of different anions ( $\text{CN}^-$ ,  $\text{AcO}^-$ ,  $\text{F}^-$ ,  $\text{Cl}^-$ ,  $\text{ClO}_4^-$  and  $\text{PF}_6^-$ ). As expected, the presence of some anions promoted a decrease in the intensity of disperse AuNPs at 530 nm and the appearance of a new peak at around 620 nm, which is consistent with an aggregation of the nanoparticles (as can be seen in the TEM Figure S1, right). This was observable to the

naked eye as a colour change from red to blue, although, as can be seen in Figure 4, both bands coexist to some extent. This is due to the addition of nucleophilic anions towards the carbocation of  $\text{MG}^+$  moiety or through the compensation of the electrostatic charges. For  $\text{CN}^-$  anions, only 180  $\mu\text{L}$  of a  $3 \times 10^{-3}$  M solution was added because the aggregation process was very fast, leading to the precipitation of the AuNP aggregates.

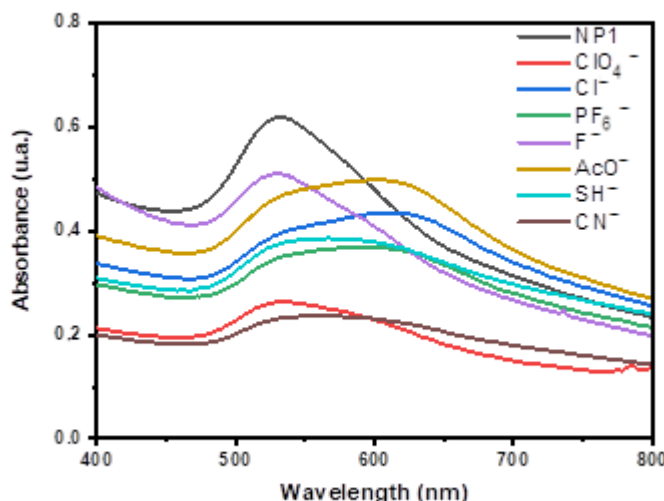


**Figure 4.** UV-vis absorption spectra of NP1 and NP1 + 300  $\mu\text{L}$  of different anions in water ( $3 \times 10^{-3}$  M).

Titration studies performed with DMF solutions of NP1 in the presence of increasing amounts of different anions are included in the Supplementary Materials. In the case of  $\text{AcO}^-$ ,  $\text{Cl}^-$  and  $\text{PF}_6^-$  anions, these changes in the spectra were concomitant with a change in the colour of the solution from red to dark blue. The variation of the ratio of the absorbance intensities of NP1 at 620 nm and 530 nm ( $A_{620}/A_{530}$ ) versus anion concentration is also presented in Figure S3 (Supplementary Materials).

The limits of detection (LOD), expressed in mol  $\text{L}^{-1}$ , were calculated from the plots of the ratio of the intensity of the absorbance at ca. 620 nm and ca. 530 ( $A_{619}/A_{530}$ ) versus anion concentration expressed in ppm (mg/L) [36] (see Table S4 in Supplementary Materials), and are shown in Table 2. Diagrams comparing the behaviour of  $\text{MG}^+$  and NP1 in the presence of different anions are shown in Figure 5.

**Table 2.** LODs of different anions with NP1.

|             | CN <sup>-</sup>       | AcO <sup>-</sup>     | F <sup>-</sup> | Cl <sup>-</sup>       | ClO <sub>4</sub> <sup>-</sup> | PF <sub>6</sub> <sup>-</sup> |
|-------------|-----------------------|----------------------|----------------|-----------------------|-------------------------------|------------------------------|
| LOD (mol/L) | $3.099 \cdot 10^{-3}$ | $5.08 \cdot 10^{-4}$ | ---            | $4.547 \cdot 10^{-4}$ | ---                           | $5.22 \cdot 10^{-4}$         |

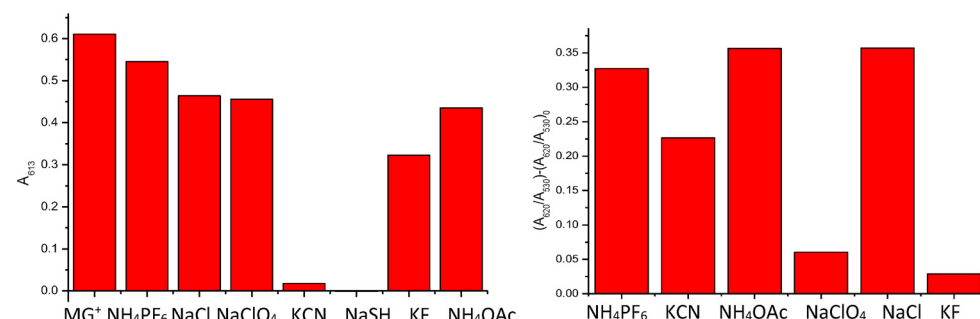


**Figure 5.** UV-vis absorbance at 619 nm of  $\text{MG}^+$  with excess of different anions (left).  $(A_{620}/A_{530}) - (A_{620}/A_{530})_0$  ratios of NP1 in the presence of different anions ( $5 \cdot 10^{-4}$  M) (right).

#### 4. Discussion

Different trends in the reactivity of monoanionic nucleophiles towards  $\text{MG}^+$  are observed when the cationic dye is free in solution and when it is attached to the surface of AuNPs. In the first case, only the stronger nucleophiles ( $\text{CN}^-$  and  $\text{HS}^-$ ) are able to react with  $\text{MG}^+$ . On the contrary, when the triaryl carbonium ion is attached to the AuNPs, it is also able to detect, with good LODs,  $\text{AcO}^-$ ,  $\text{Cl}^-$  and  $\text{PF}_6^-$ . It is not clear whether a reaction or a charge compensation process, leading to aggregation of the Nps, is responsible. However, a modification of the electrophilicity of the supported cation is likely, as only the hard nucleophiles  $\text{ClO}_4^-$  and  $\text{F}^-$  do not promote the aggregation.

#### 5. Conclusions

In summary, we have synthesized  $\text{MG}^+$ -functionalized AuNPs, NP1, for the detection of anions. The detection process is based on the compensation of the positive charges at the surface of the nanoparticles, which triggers their aggregation, resulting in a bathochromic shift in the plasmon resonance band. A different electrophilicity capacity is observed for the carbocation in solution or linked to the AuNPs, which made it possible to distinguish the nucleophilic character of different anions. Only the strong and soft nucleophile anions such as cyanide and hydrogen sulphide decolorate malachite green in DMF solution. However, when a malachite green derivative is anchored to AuNPs, fewer nucleophilic anions are able to promote aggregation, except for hard nucleophiles such as  $\text{ClO}_4^-$  and  $\text{F}^-$ .

**Supplementary Materials:** The following supporting information can be downloaded at: <https://www.mdpi.com/article/10.3390/colorants2040030/s1>; Figure S1: TEM images of NP1 and aggregated NP1; Figure S2: UV-vis spectra of the  $\text{MG}^+$  on addition of increasing amounts of KCN and NaSH; Figure S3: UV-vis spectra of the NP1 on addition of increasing amounts of anions expressed; Table S4: Determination of the LODs.

**Author Contributions:** Conceptualization and investigation, J.A.S. and P.G.; methodology, A.M.; software, validation and formal analysis, P.A.; resources and writing—original draft preparation, S.G. and M.P. All authors have read and agreed to the published version of the manuscript.

**Funding:** The authors gratefully acknowledge grant PID2021-126304OB-C42 funded by the Spanish MCIN/AEI/10.13039/501100011033 and by “ERDF A way of making Europe, EU”.

**Institutional Review Board Statement:** Not applicable.

**Informed Consent Statement:** Not applicable.

**Data Availability Statement:** Data is contained within the article or Supplementary Material.

**Acknowledgments:** SCSIE (Universitat de Valencia) is gratefully acknowledged for all the equipment employed. NMR was registered at the U26 facility of ICTS “NAMBIOSIS” at the Universitat of València.

**Conflicts of Interest:** The authors declare no conflict of interest.

#### References

1. Swain, G.; Scott, C.B. Quantitative Correlation of Relative Rates. Comparison of Hydroxide Ion with Other Nucleophilic Reagents toward Alkyl Halides, Esters, Epoxides and Acyl Halides. *J. Am. Chem. Soc.* **1953**, *75*, 141–147. [[CrossRef](#)]
2. Ritchie, C.D. Nucleophilic reactivities toward cations. *Acc. Chem. Res.* **1972**, *5*, 348–354. [[CrossRef](#)]
3. Mayr, H.; Ofial, A.R. Do general nucleophilicity scales exist? *J. Phys. Org. Chem.* **2008**, *21*, 584–595. [[CrossRef](#)]
4. Mayr, H.; Patz, M. Scales of Nucleophilicity and Electrophilicity: A System for Ordering Polar Organic and Organometallic Reactions. *Angew. Chem. Int. Ed. Engl.* **1994**, *33*, 938–957. [[CrossRef](#)]
5. Parr, R.G.; Szentpály, L.V.; Liu, S. Electrophilicity Index. *J. Am. Chem. Soc.* **1999**, *121*, 1922–1924. [[CrossRef](#)]
6. Kiyooka, S.-I.; Kaneno, D.; Fujiyama, R. Intrinsic reactivity index as a single scale directed toward both electrophilicity and nucleophilicity using frontier molecular orbitals. *Tetrahedron* **2013**, *69*, 4247–4258. [[CrossRef](#)]
7. Jaramillo, P.; Pérez, P.; Contreras, R.; Tiznado, W.; Fuentealba, P. Definition of a Nucleophilicity Scale. *J. Phys. Chem. A* **2006**, *110*, 8181–8187. [[CrossRef](#)]
8. Liu, S.; Rong, C.; Lu, T. Information Conservation Principle Determines Electrophilicity, Nucleophilicity, and Regioselectivity. *J. Phys. Chem. A* **2014**, *118*, 3698–3704. [[CrossRef](#)]

9. Martí, A.; Costero, A.M.; Gaviña, P.; Parra, M. Triarylcarbinol functionalized gold nanoparticles for the colorimetric detection of nerve agent simulants. *Tetrahedron Lett.* **2014**, *55*, 3093–3096. [[CrossRef](#)]
10. Xi, C.; Liu, Z.; Kong, L.; Hu, X.; Liu, S. Effects of interaction of folic acid with uranium (VI) and basic triphenylmethane dyes on resonance Rayleigh scattering spectra and their analytical applications. *Anal. Chim. Acta* **2008**, *613*, 83–90. [[CrossRef](#)]
11. Eldem, Y.; Özer, I. Electrophilic reactivity of cationic triarylmethane dyes towards proteins and protein-related nucleophiles. *Dye. Pigment.* **2004**, *60*, 49–54. [[CrossRef](#)]
12. Cho, P.; Yang, T.; Blankenship, L.R.; Moody, J.D.; Churchwell, M.; Beland, F.A.; Culp, S.J. Synthesis and Characterization of N-Demethylated Metabolites of Malachite Green and Leucomalachite Green. *Chem. Res. Toxicol.* **2003**, *16*, 285–294. [[CrossRef](#)] [[PubMed](#)]
13. Jang, M.-S.; Kang, N.-Y.; Kim, K.-S.; Kim, C.-H.; Lee, J.-H.; Lee, Y.-C. Mutational analysis of NADH-binding residues in triphenylmethane reductase from Citrobacter sp. strain KCTC 18061P. *FEMS Microbiol. Lett.* **2007**, *271*, 78–82. [[CrossRef](#)] [[PubMed](#)]
14. Soborover, E.I.; Tverskoi, V.A.; Tokarev, S.V. An optical chemical sensor based on functional polymer films for controlling sulfur dioxide in the air of the working area: Acrylonitrile and alkyl methacrylate copolymers with brilliant green styrene sulfonate. *J. Anal. Chem.* **2005**, *60*, 274–281. [[CrossRef](#)]
15. Motomizu, S.; Fujiwara, S.; Toei, K. Liquid—Liquid distribution behavior of ion-pairs of triphenylmethane dye cations and their analytical applications. *Anal. Chim. Acta* **1980**, *128*, 185–194. [[CrossRef](#)]
16. Uda, R.M.; Oue, M.; Kimura, K. Specific behavior of crowned crystal violet in cation complexation and photochromism. *J. Supramol. Chem.* **2002**, *2*, 311–316. [[CrossRef](#)]
17. Kimura, K.; Mizutani, R.; Yokoyama, M.; Arakawa, R.; Sakurai, Y. Metal-Ion Complexation and Photochromism of Triphenylmethane Dye Derivatives Incorporating Monoaza-15-crown-5 Moieties. *J. Am. Chem. Soc.* **2000**, *122*, 5448–5454. [[CrossRef](#)]
18. Dickert, F.L.; Vonend, M.; Kimmel, H.; Mages, G. Dyes of the triphenylmethane type as sensor materials for solvent vapours. *Fresenius' Z. Anal. Chem.* **1989**, *333*, 615–618. [[CrossRef](#)]
19. Bengtesson, G. Acta Chem Scand—Consistent data. *Acta Chem. Scand.* **1969**, *23*, 455–466. [[CrossRef](#)]
20. Gupta, S.K.S.; Mishra, S.; Rani, V.R. A study on equilibrium and kinetics of carbocation-to-carbinol conversion for di- and triarylmethane dye cations in aqueous solutions: Relative stabilities of dye carbocations and mechanism of dye carbinol formation. *Indian J. Chem. Sec. A* **2000**, *39*, 703–708.
21. Chen, Y.-C.; Lee, I.-L.; Sung, Y.-M.; Wo, S.-P. Triazole functionalized gold nanoparticles for colorimetric Cr<sup>3+</sup> sensing. *Sensors Actuators B Chem.* **2013**, *188*, 354–359. [[CrossRef](#)]
22. Li, H.; Yong, Y.-W. Gold nanoparticles functionalized with supramolecular macrocycles. *Chin. Chem. Lett.* **2013**, *24*, 545–552. [[CrossRef](#)]
23. Knighton, R.C.; Sambrook, M.R.; Vincent, J.C.; Smith, S.A.; Serpell, C.J.; Cookson, J.; Vickers, M.S.; Beer, P.D. Fluorogenic dansyl-ligated gold nanoparticles for the detection of sulfur mustard by displacement assay. *Chem. Commun.* **2013**, *49*, 2293–2295. [[CrossRef](#)] [[PubMed](#)]
24. Kumar, V.; Anslyn, E.V. A Selective Turn-On Fluorescent Sensor for Sulfur Mustard Simulants. *J. Am. Chem. Soc.* **2013**, *135*, 6338–6344. [[CrossRef](#)] [[PubMed](#)]
25. Wang, A.-J.; Guo, H.; Zhang, M.; Zhou, D.-L.; Wang, R.-Z.; Feng, J.-J. Sensitive and selective colorimetric detection of cadmium(II) using gold nanoparticles modified with 4-amino-3-hydrazino-5-mercaptop-1,2,4-triazole. *Microchim. Acta* **2013**, *180*, 1051–1057. [[CrossRef](#)]
26. Rastegarzadeh, S.; Rezaei, Z.B. Environmental assessment of 2-mercaptobenzimidazole based on the surface plasmon resonance band of gold nanoparticles. *Environ. Monit. Assess.* **2013**, *185*, 9037–9042. [[CrossRef](#)]
27. Mayer, K.M.; Hafner, J.M. Localized Surface Plasmon Resonance Sensors. *Chem. Rev.* **2011**, *111*, 3828–3857. [[CrossRef](#)]
28. Jiang, Y.; Wang, Y.; Ma, N.; Wang, Z.; Smet, M.; Zhang, X. Reversible Self-Organization of a UV-Responsive PEG-Terminated Malachite Green Derivative: Vesicle Formation and Photoinduced Disassembly. *Langmuir* **2007**, *23*, 4029–4034. [[CrossRef](#)]
29. Barghouthi, Z.; Amereih, S. Spectrophotometric determination of fluoride in drinking water using aluminium complexes of triphenylmethane dyes. *Water SA* **2012**, *38*, 543–548. [[CrossRef](#)]
30. Reuben, D.M.E.; Bruice, T.C. Reaction of thiol anions with benzene oxide and malachite green. *J. Am. Chem. Soc.* **1976**, *98*, 114–121. [[CrossRef](#)]
31. Kaur, P.; Sareen, D.; Kaur, S.; Singh, K. An efficacious “naked-eye” selective sensing of cyanide from aqueous solutions using a triarylmethane leuconitrile. *Inorg. Chem. Commun.* **2009**, *12*, 272–275. [[CrossRef](#)]
32. Haiss, W.; Thanh, N.T.K.; Aveyard, J.; Fernig, D.G. Determination of Size and Concentration of Gold Nanoparticles from UV–Vis Spectra. *Anal. Chem.* **2007**, *79*, 4215–4221. [[CrossRef](#)] [[PubMed](#)]
33. Kong, B.; Zhu, A.; Luo, Y.; Tian, Y.; Yu, Y.; Shi, G. Sensitive and Selective Colorimetric Visualization of Cerebral Dopamine Based on Double Molecular Recognition. *Angew. Chem. Int. Ed.* **2011**, *50*, 1837–1840. [[CrossRef](#)] [[PubMed](#)]
34. Godoy-Reyes, T.M.; Costero, A.M.; Gaviña, P.; Martínez-Máñez, R.; Sancenón, F. Colorimetric detection of normetanephrine, a pheochromocytoma biomarker, using bifunctionalised gold nanoparticles. *Anal. Chim. Acta* **2019**, *1056*, 146–152. [[CrossRef](#)]
35. Martí, A.; Costero, A.M.; Gaviña, P.; Gil, S.; Parra, M.; Brotons-Gisbert, M.; Sánchez-Royo, J.F. Functionalized Gold Nanoparticles as an Approach to the Direct Colorimetric Detection of DCNP Nerve Agent Simulant. *Eur. J. Org. Chem.* **2013**, *2013*, 4770–4779. [[CrossRef](#)]
36. Liu, B.; Wang, H.; Wang, T.; Bao, Y.; Du, F.; Tian, J.; Li, Q.; Bai, R. A new ratiometric ESIPT sensor for detection of palladium species in aqueous solution. *Chem. Commun.* **2012**, *48*, 2867–2869. [[CrossRef](#)]